

LONG-TERM X-RAY MONITORING OF THE YOUNG PULSAR PSR B1509–58

MARGARET A. LIVINGSTONE¹, VICTORIA M. KASPIDepartment of Physics, Rutherford Physics Building, McGill University, 3600 University Street, Montreal, Quebec, H3A 2T8, Canada
Draft version February 18, 2022

ABSTRACT

It has long been thought that the pulsed X-ray properties of rotation-powered pulsars are stable on long time scales. However, long-term, systematic studies of individual sources have been lacking. Furthermore, dramatic X-ray variability has now been observed from two pulsars having inferred sub-critical dipole magnetic fields. Here we present an analysis of the long-term pulsed X-ray properties of the young, energetic pulsar PSR B1509–58 using data from the *Rossi X-ray Timing Explorer*. We measured the 2–50 keV pulsed flux for 14.7 yr of X-ray observations and found that it is consistent with being constant on all relevant time scales, and place a 3σ upper limit on day-to-week variability of $<28\%$. In addition, we searched for magnetar-like X-ray bursts in all observations and found none, which we use to constrain the measurable burst rate to less than one per 750 ks of observations. We also searched for variability in the pulse profile and found that it is consistent with being stable on time scales of days to decades. This supports the hypothesis that X-ray properties of rotation-powered X-ray pulsars can be stable on decade-long time scales. In addition, we extend the existing timing solution by 7.1 yr to a total of 28.4 yr and report updated values of the braking index, $n = 2.832 \pm 0.003$ and the second braking index, $m = 17.6 \pm 1.9$.

Subject headings: pulsars: individual (PSR B1509–58), supernovae: individual (G320.4–1.2)

1. INTRODUCTION

The X-ray emission properties of non-accreting neutron stars are today known to be extremely diverse. There are multiple classes of neutron stars identified – rotation-powered pulsars (RPPs), Anomalous X-ray Pulsars (AXPs), Soft Gamma Repeaters (SGRs), thermally emitting isolated neutron stars, central compact objects – to name a few (see Kaspi 2010, for a review), with the basis for classification of a given neutron star into these different classes often being its X-ray emission properties.

Anomalous X-ray Pulsars (AXPs) and Soft Gamma Repeaters (SGRs) are now well established as being extremely variable in the X-ray range, showing a wide variety of often dramatic bursting behavior during active periods, in addition to lower-level flux and profile variability during periods of relative quiescence (see Woods & Thompson 2006, Kaspi 2007, Mereghetti 2008, and Rea & Esposito 2011, for reviews). This variability is ascribed to activity both within the stellar interior as well as in the magnetosphere, both owing ultimately to the decay of these objects’ extremely high magnetic fields ($B > B_{QED} \equiv 4.4 \times 10^{13}$ G), particularly in the context of the now widely accepted magnetar model (Thompson & Duncan 1996; Thompson et al. 2002).

Interestingly, two recent results have lowered the estimated dipolar field strength necessary for magnetar-like activity to well below $B \simeq 10^{14}$ G (e.g. Thompson et al. 2002). The young RPP PSR J1846–0258 with $B = 4.9 \times 10^{13}$ G experienced a magnetar-like outburst in 2006 (Gavril et al. 2008; Kumar & Safi-Harb 2008), while the SGR 0418+5729, discovered via an outburst in 2009, has an upper limit on its dipole field of $B < 7.5 \times 10^{12}$ G (Rea et al. 2010). Thus, the smallest possible B field needed to power a magnetar-like outburst is not cur-

rently known. These recent discoveries highlight the fact that the link between magnetars and RPPs is poorly understood. In particular, it suggests that the X-ray emission of some RPPs may be more variable than previously thought. Indeed, a study by Perna & Pons (2011) argues that bursting behavior may be generically possible in all RPPs, only more common in those that are young and with high B .

Systematic examinations of the X-ray variability properties of RPPs in order to look for other examples of bursting behavior or flux changes has been hampered by the difficulty in obtaining a well sampled data set with a single, well calibrated instrument over a long time span. Rotation-powered pulsars are generally too faint for detection with all-sky monitors.

PSR B1509–58 is a young, energetic pulsar that was discovered with the *Einstein* satellite (Seward & Harnden Jr. 1982). It has period 150 ms, a high spin-down luminosity of $\dot{E} = 1.7 \times 10^{37}$ erg s^{−1}, and a relatively large inferred² dipolar magnetic field of $B = 1.5 \times 10^{13}$ G, larger than that for the magnetar with the smallest estimate of $B < 7.5 \times 10^{12}$ G (Rea et al. 2010). PSR B1509–58’s high spin-down rate and lack of glitches have allowed the measurement of higher-order spin parameters, in particular, the second and third frequency derivatives ($\ddot{\nu}$ and $\dddot{\nu}$). These provide a determination of the braking index, $n = \nu\ddot{\nu}/\dot{\nu}^2 = 2.839 \pm 0.003$, and second braking index, $m = \nu^2\ddot{\nu}/\dot{\nu}^3 = 18.3 \pm 2.9$ (Kaspi et al. 1994; Livingstone et al. 2005b), allowing tests of the standard pulsar spin-down model (e.g. Blandford 1994).

PSR B1509–58 presents an excellent opportunity for a systematic, long-term study of a RPP’s X-ray emission

¹ maggie@physics.mcgill.ca² Note that the dipolar magnetic field for pulsars is $B = 3.2 \times 10^{19} \sqrt{P\dot{P}}$ G.

properties, since it has been observed regularly since 1996 with the Proportional Counter Array (PCA) aboard the *Rossi X-ray Timing Explorer (RXTE)* as a timing calibration source. Here we present a search of 14.7 yr of *RXTE* data of PSR B1509–58 for pulsed flux variations, pulse profile variations, and magnetar-like bursts. We also extend the timing solution for the pulsar by 7.1 yr, increasing the total observing time to 28.4 yr. We use these new data to refine the measurements of n and m , and further quantify the variability of n .

2. OBSERVATIONS

PSR B1509–58 data were obtained with the Proportional Counter Array (PCA; Jahoda et al. 1996; Jahoda et al. 2006) on board *RXTE*. The PCA consists of five collimated xenon/methane multi-anode proportional counter units (PCUs) operating in the 2–60 keV range, with a total effective area of approximately 6500 cm² and a field of view of $\sim 1^\circ$ FWHM. We downloaded 290 archival *RXTE* observations of PSR B1509–58 from the HEASARC archive³. All data were collected in the GoodXenon mode, which records the arrival time (1 μ s resolution) and energy (256 channel resolution) of each unrejected event. The observations span 7.1 yr from MJD 50148–55221 (1996 March 6 – 2010 November 21).

The data reduction and preparation is significantly different for the timing and pulse profile analyses than for the pulsed flux analysis. Details for each are included in the following sections.

3. TIMING ANALYSIS

Our timing analysis of PSR B1509–58 follows the common phase-coherent approach, in which we account for each rotation of the pulsar. Pulse times of arrival are fitted with a Taylor expansion of pulse phase (see, for example, Manchester & Taylor 1977), allowing the extraction of precise spin parameters (spin-frequency ν , and frequency derivatives $\dot{\nu}$, $\ddot{\nu}$, and $\dddot{\nu}$).

In order to produce pulse times-of-arrival (TOAs), we extracted photons from all three xenon layers of each PCU in the 2 – 30 keV energy range (or 4 – 72 channel range). Data from the individual PCUs were merged and binned at 1/1024s resolution. The time series were reduced to barycentric dynamical time (TDB) at the solar system barycenter using the known position from radio interferometry (J2000 RA = 15^h 13^m 55^s.62, Dec = –59° 08′ 9.00″; Gaensler et al. 1999) and the JPL DE200 solar system ephemeris.

When more than one observation occurred in a 24-hr period, we combined the data from multiple observations into a single time series in order to produce better TOAs and having smaller uncertainties. Each time series was folded with 64 phase bins using an initial ephemeris from Livingstone et al. (2005b). Resulting pulse profiles were cross-correlated in the Fourier domain with a high signal-to-noise-ratio template. We implemented a Fourier domain filter by using six harmonics in the cross-correlation procedure. Cross-correlation produces an average TOA for each observation with a typical uncertainty of ~ 0.5 ms. TOAs were fitted phase coherently

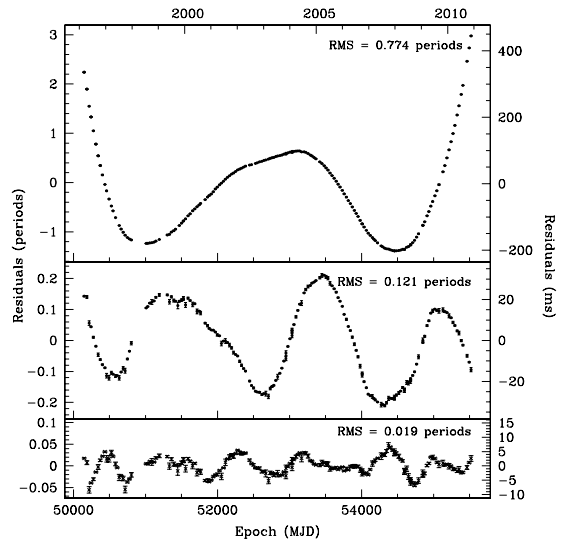


Figure 1. *RXTE* timing residuals for PSR B1509–58 spanning 1996 March – 2010 November. The top panel has ν , $\dot{\nu}$, and $\ddot{\nu}$ fitted; the middle panel has a quartic polynomial (i.e. $\ddot{\nu}$ fitted), and the bottom panel has 12 derivatives fitted. Spin parameters from a fully phase-coherent fit are given in Table 1.

with the pulse timing software package *TEMPO*⁴; timing residuals and refined spin parameters are produced as output. Spin parameters for all 14.7 yr of X-ray data are given in Table 1.

The top panel of Figure 1 shows timing residuals with pulse frequency, ν , frequency derivative, $\dot{\nu}$, and second frequency derivative, $\ddot{\nu}$, fitted. No sudden jumps were found during the phase connection process, nor were any cusps identified in the timing residuals, indicating that no glitches occurred during the time spanned by the *RXTE* observations. The middle panel shows residuals with $\ddot{\nu}$ also fitted. PSR B1509–58 is one of two pulsars with deterministic measurements of $\ddot{\nu}$ and $\dddot{\nu}$ (Kaspi et al. 1994; Livingstone et al. 2005b), however, after the removal of all deterministic parameters, significant structure remains in the timing residuals, as is visible in the middle panel. This can be attributed to timing noise, a low-frequency or “red” noise process that is a common but poorly understood phenomenon in pulsars (and previously discussed in detail for this pulsar in Livingstone et al. 2005b). *TEMPO* has the capability to fit up to 12 frequency derivatives; the results of this fit are shown in the bottom panel of Figure 1. The presence of timing noise is known to contaminate measurements of higher order spin parameters such as n and m and complicates the proper estimation of uncertainties. One method of measuring deterministic parameters and estimating their true uncertainties in the presence of timing noise is discussed in the following section.

3.1. Partially phase-coherent timing analysis

One method of finding reliable values for n and m in the presence of timing noise is to use a piece-wise approach, deemed “partially coherent” timing analysis. The data are broken into subsets, each of which is fitted phase-coherently with ν , $\dot{\nu}$, and $\ddot{\nu}$. For each subset, we require that no structure be visible in the resulting timing

³ <http://heasarc.gsfc.nasa.gov/docs/archive.html>

⁴ www.atnf.csiro.au/people/pulsar/tempo/

residuals. The amount of data included in each subset is determined only by this requirement, so is allowed to vary. On average, the time span in a subset is ~ 500 days. The date ranges spanned by these subsets and the resulting ephemerides are given in Table 2 (and are used for our pulsed flux analysis, see Section 4). In order to better sample the available data, we created additional subsets that overlapped the original subsets by $\sim 1/2$. Overlapping subsets are useful since short coherent timing solutions produce fitted parameters dominated by the end points (e.g. Livingstone et al. 2005b). Figure 5 shows all measurements of $\ddot{\nu}$ both from the current analysis, as well as previous measurements determined using the same method but from both radio and X-ray timing data reported in Livingstone et al. (2005b).

We performed a weighted least squares fit to measure $\ddot{\nu}$ and a bootstrap error analysis to better estimate the uncertainties, since the data are known to be contaminated with red noise leading to formal uncertainties that underestimate the true uncertainties (Efron 1979). This analysis results in $\ddot{\nu} = -1.21(13) \times 10^{-31} \text{ s}^{-4}$, in agreement with the previously reported value of $\ddot{\nu} = -1.28(21) \times 10^{-31} \text{ s}^{-4}$, based on 21.3 yr rather than 28.4 yr of data, but calculated in the same way.

A value of $\ddot{\nu}$ can be used to find a measurement of the “second” braking index, m , via $m = \nu^2 \ddot{\nu} / \dot{\nu}^3$. This parameter, a higher order analog to the braking index, n , provides a unique test of pulsar spin-down models (e.g. Blandford & Romani 1988). The above value of $\ddot{\nu}$ corresponds to a value of $m = 17.6 \pm 1.9$, smaller than the value from 21.3 yr of data reported in Livingstone et al. (2005b) of $m = 18.3 \pm 2.9$, but not significantly so.

We used the same timing solutions to calculate n for each data subset as shown in Figure 2. The weighted average value, with the uncertainty calculated from a bootstrap analysis is $n = 2.832 \pm 0.003$, smaller than the previously reported value of 2.839 ± 0.003 at the 1.6σ level. In order to look for a linear change in n over the entire 28.4 yr of observations, we performed a weighted linear least squares fit to the data. This results in a slope of $\Delta n / \Delta t = (-4 \pm 2) \times 10^{-6}$, which is consistent with no secular change in n at the 2σ level. While the long-term n is relatively stable, short-term variability is visible as scatter in the individual measurements, which can most likely be attributed to timing noise, since no discrete jumps in ν , i.e. glitches, were found. This amounts to a maximum variation from the average value of $4.8 \pm 0.3\%$, and a root-mean-square variation from the mean of 3.5% . Because of the large scatter in the measurement of $\ddot{\nu}$ near MJD 55000, which is significantly larger than the mean, we further verified that no glitch occurred in this time period.

4. PULSED FLUX ANALYSIS AND RESULTS

In order to determine the pulsed flux of PSR B1509–58 at each epoch, for each observation, we created a phase resolved spectrum with 8 phase bins, for each PCU. Each observation was folded with the software package **fasebin**⁵ using the appropriate short coherent ephemeris described in Section 3.1 and listed in Table 2. We used these short ephemerides instead of the global solution in part because **fasebin** can take a maximum

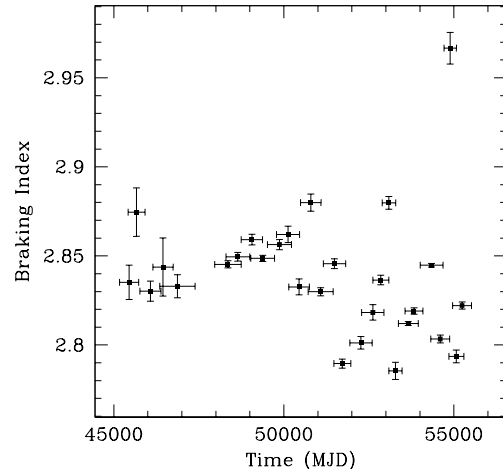


Figure 2. Braking indices from short phase-coherent timing solutions. Data prior to MJD 53000 were previously reported in (Livingstone et al. 2005b). The weighted average is $n = 2.832 \pm 0.003$. At the 2σ level, there is no linear change over 28.4 yr. Significant scatter is apparent in the data; the root-mean square variation from the mean n is at the 3.5% -level.

of two frequency derivatives for an input ephemeris. For PSR B1509–58, using the global two-derivative ephemeris produces very poor pulse profiles because of the effect of the deterministic $\ddot{\nu}$ and timing noise, whereas the profiles produced from short ephemerides are consistently good. A phase-averaged spectrum was also created in order to build a response matrix for each PCU. For each observation, we combined phase-resolved spectra and response matrices for all PCUs that were on for $> 95\%$ of the observation.

From each combined phase-resolved spectrum, we created a pulse profile with 8 phase bins in the 2–50 keV energy range. The minimum bin of each profile was used to set the background level, and was subtracted from all bins of the phase-resolved profile.

After background subtraction, we combined the spectra for all phase bins into a single spectrum and fitted the result using **XSPEC**⁶. For each observation, we used a simple power-law model with a fixed spectral index of $\Gamma = 1.19$ and fixed $N_H = 8.6 \times 10^{21} \text{ cm}^{-2}$ (Cusumano et al. 2001), fitting only for the flux. The resulting fit χ^2 values showed that this model fit all of our data well.

For short exposure times, there is an observed anti-correlation between the measured pulsed flux and the source exposure time. This is a statistical effect present for all sources and disappears when sufficient counts are detected, i.e. for longer exposure times. While one might expect that the uncertainties on pulsed flux measurements would simply increase for short exposures, in addition, the measured pulsed flux is biased upwards. This arises from Poissonian variations, which lead to the minimum bin being biased downward when there are few total counts, thus to an under-estimate of the background and an over-estimate of the pulsed flux. Because the number of active PCUs changes from observation to observation, for convenience, we define an “effective” observation time of $T_{\text{eff}} = N_{\text{pcus}} T_{\text{obs}}$, where N_{pcus} is the number of PCUs

⁵ <http://heasarc.nasa.gov/docs/xte/recipes/fasebin.html>

⁶ <http://xspec.gsfc.nasa.gov/> Version 11.3.1

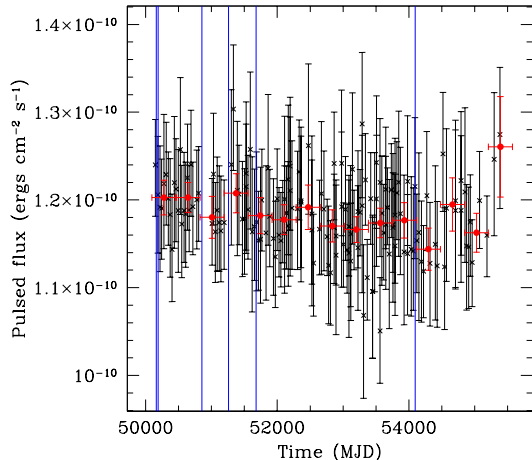


Figure 3. Absorbed pulsed flux measurements for PSR B1509–58 determined for observations with $T_{\text{eff}} > 6$ ks. Vertical lines mark dates of epoch changes in *RXTE*. Filled circles (colored red in the online version) show the average pulsed flux over year-long periods. The average pulsed flux in the 2–50 keV energy range is $1.181(5) \times 10^{-13} \text{ erg cm}^{-2} \text{ s}^{-1}$. A weighted least-squares fit to the data gives a slope of $(-7.4 \pm 3.8) \times 10^{-16} \text{ erg cm}^{-2} \text{ s}^{-1} \text{ day}^{-1}$, indicating that the pulsed flux is consistent with having no linear trend at the 1.9σ level.

on during an observation and T_{obs} is the on-source time. We compared the measured flux values to T_{eff} and found a small bias to be present. This bias was eliminated by excluding all observations having $T_{\text{eff}} < 6$ ks, which amounts to 34% of the data.

Figure 3 shows all measurements of the pulsed component of the flux of PSR B1509–58 for observations with $T_{\text{eff}} > 6$ ks. Vertical lines delimit each of the *RXTE* epochs (1, 2, 3, 3a, 4) and the losses of the propane layers in PCU0 (also referred to as epoch 5) and PCU1⁷. We verified that there are no significant correlations between the pulsed flux and any of the gain changes or propane layer loss events. We also measured the pulsed count rate for each observation and note that correlations exist between the pulsed count rate and gain changes and propane layer losses. In addition, the pulsed count rate decreases gradually by $\sim 10\%$ over the lifetime of *RXTE*, associated with the long-term degradation of the PCA. For these reasons, we report only the pulsed flux values, despite somewhat larger uncertainties. We note that PSR B1509–58 is listed as a calibration source for *RXTE* but has only been used as a timing calibrator and not a flux calibration source⁸.

The weighted average 2–50 keV absorbed pulsed flux for all 14.7 yr is $1.181(5) \times 10^{-10} \text{ erg cm}^{-2} \text{ s}^{-1}$, with a χ^2 value of 52.4 for 150 degrees of freedom. A weighted linear least-squares fit to the pulsed flux values f gives $\Delta f / \Delta t = (-7.4 \pm 3.8) \times 10^{-16} \text{ erg cm}^{-2} \text{ s}^{-1} \text{ day}^{-1}$, that is, consistent with having no linear trend at the 1.9σ level. The maximum variation of the pulsed flux of a single observation from the average corresponds to a variability of $(10 \pm 6)\%$. At the 3σ level, we can rule out changes on day-to-week time scales of greater than 28% from the average pulsed flux value. We also studied the

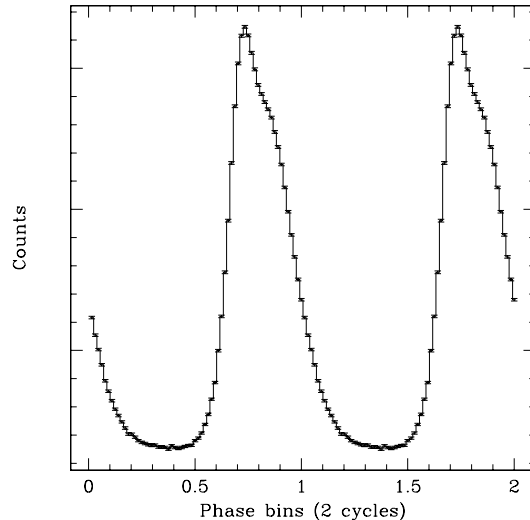


Figure 4. Summed 64-bin pulse profile for PSR B1509–58 for all 14 Cycles of *RXTE* data for the 2–50 keV energy range. We found no significant difference between individual pulse profiles and the average template, as discussed in Section 5.

flux stability on monthly and yearly time scales by creating weighted averages of individual flux measurements. Average flux values for each *RXTE* cycle are shown on Figure 3 as filled circles (colored red in the online version). On monthly time scales, at the 3σ level, we rule out variation from the average larger than 20%, while on yearly time scales, the 3σ upper limit on variability is 21%.

5. PULSE PROFILE ANALYSIS

In order to search for variability in the X-ray pulse profile of PSR B1509–58, we folded each 2–30 keV time series (as described for the timing analysis in Section 3) with the appropriate ephemeris given in Table 2. Previous studies have examined the pulse profile as a function of energy in detail and found that the pulse shape does not change appreciably in the *RXTE* energy range (Rots et al. 1998; Marsden et al. 1997), hence we do not repeat this analysis here and concentrate instead on the possibility of the profile changing with time.

First, we analyzed the profiles for individual observations in order to search for variability on time scales of days to months (i.e. the range of time spans between individual observations). We created a template profile by summing all aligned pulse profiles, shown in Figure 4. We subtracted a DC offset from both the individual profiles and template, then normalized the template to each individual profile, subtracted them and found the residuals between the two profiles. We calculated the reduced χ^2 of the resulting residuals and in each case, we see no evidence for pulse profile variability. To quantify the lack of profile changes, we calculated the root-mean-square of the profile residuals as a percentage of the number of counts in each DC-offset subtracted profile and found a 3σ upper limit on variations of 2.1%.

Next, we created a single profile for each *RXTE* observing cycle (spanning ~ 1 -yr each). In order to check whether there were any small-scale changes in the pulse profile, we compared each profile against the previously described template profile. Repeating the analysis de-

⁷ http://heasarc.gsfc.nasa.gov/docs/xte/pca_history.html
<http://heasarc.gsfc.nasa.gov/docs/xte/e-c-table.html>

⁸ See, for example, <http://heasarc.gsfc.nasa.gov/docs/xte/abc/time.html>

scribed above, again we found no evidence for variability. For the yearly profiles, we found a 3σ upper limit on profile changes of less than 0.1%.

We also compared the profile from each of the 14 *RXTE* cycles with that of the previous and subsequent cycle profiles. We normalized each profile and then created residuals between pairs of profiles. We then performed a χ^2 test on each set of residuals. In every case, $\chi^2_\nu < 1$, i.e. we detected no evidence of long term changes in the pulse profile. In order to have maximum sensitivity to changes on the longest possible time scales, we also repeated the analysis by comparing the Cycle 1 profile with the Cycle 14 profile. Again, we found that $\chi^2_\nu < 1$.

6. BURST SEARCH

To search for magnetar-like X-ray bursts from PSR B1509–58, for each observation we created a time series for each active PCU from GoodXenon data, selecting events in the 2 – 20 keV range and from all three detection layers (the same energy range as selected for similar searches for X-ray bursts from AXPs, e.g. Gavril et al. 2004). This was repeated several times with different time resolutions, specifically for 15.625 ms, 31.25 ms, 62.5 ms and 125 ms, to provide sensitivity to bursts on a hierarchy of time scales. The procedure used here was based on that described in Gavril et al. (2004).

By this algorithm, bursts are identified by comparing the count rate in the i^{th} bin to the average count rate. Because the background rate of the PCA typically varies over a single observation, we calculated a local mean around the i^{th} bin. We then compared the count rate in the i^{th} bin to the local average. If the count rate in a single bin was larger than the local average, the probability of such a count rate occurring by chance was calculated. Then the probability of the count rate in the corresponding bin in the other active PCUs was also calculated (whether or not the count rate in that bin was greater than the local average). If a PCU was off during the bin of interest, its probability was set to 1. We then found the total probability that a burst was observed. If the total probability of an event was $P_{i,\text{tot}} \leq 0.01/N$ (where N is the total number of time bins searched), it was flagged as a burst.

We searched a total of 751 ks of *RXTE* data using the above described process and found no X-ray bursts from the direction of PSR B1509–58.

Unlike the AXPs, PSR B1509–58 has a bright PWN which contributes a large unpulsed background to the 1° field-of-view of the PCA. Because of this larger background, the sensitivity to AXP-like X-ray bursts could be significantly smaller than for the AXPs. Thus, in order to determine the fluence of bursts that would have been detectable in these data, we added simulated bursts to real *RXTE* time series of PSR B1509–58. Each simulated burst was confined to a single time bin and spread between the operational PCUs. We added many bursts to each time series, each separated by sufficient time that only one burst would ever be included in a calculation of the running mean. Many bursts were added to each time series in order to include the effect of the variation of the background count rate, largely owing to the variable particle background during the *RXTE* orbit. We repeated this analysis for each time resolution searched.

Unsurprisingly, we found that the minimum burst fluence required to detect 100% of the simulated bursts is a function of both the number of operational PCUs and width of the time bins.

In terms of detected burst count rates, the smallest detectable bursts are similar to the smallest bursts detected from the AXP 1E 2259+586 in its large 2002 outburst (Gavril et al. 2004). For example, for 31.25 ms time resolution, 100% of simulated bursts are detected if the burst consisted of 8 or more counts per PCU or more than 25 counts/burst total (i.e. at least 25 counts per 31.35 ms time bin). In order to quantify this in terms of burst fluences, we assumed a burst spectrum of a simple power law with spectral index of $\Gamma = 1.35$, as measured for the 80 bursts found from the AXP 1E 2259+586 (Gavril et al. 2004). For 62.5 ms time resolutions, we found that burst fluences of $\geq 1.5 \times 10^{-11}$ erg cm $^{-2}$ (2–20 keV) would have been detected, an order of magnitude less than the smallest burst fluence detected from PSR J1846–0258 in its 2006 outburst (Gavril et al. 2008). Detectable burst rates and fluences for all searched time resolutions are given in Table 3, and are valid in the absence of instrumental flares. Thus, we can confidently exclude the possibility that AXP-like X-ray bursts with fluences larger than the limits given in Table 3 were present in the *RXTE* PSR B1509–58 data.

7. DISCUSSION

We searched for several types of X-ray variability from the young, high- B field pulsar PSR B1509–58 and found that the pulsar is stable in each way studied. This establishes a baseline for the quiescent pulsed flux of PSR B1509–58 in case of a future magnetar-like outburst. We establish a 3σ upper limit on pulsed flux variations of less than 28% from the average, ruling out pulsed flux changes similar to those seen in the magnetars and PSR J1846–0258. For example, during the 2006 outburst of PSR J1846–0258, the 2–60 keV pulsed flux as measured with *RXTE* increased by a factor of ~ 3 (Gavril et al. 2008).

The burst search algorithm that has successfully discovered X-ray bursts from several AXPs and PSR J1846–0258 did not reveal any bursts from the direction of PSR B1509–58. We searched 751 ks of *RXTE* observations for X-ray bursts, implying that the burst rate must be less than one burst per 751 ks. This is less than the burst rate for PSR J1846–0258, where 5 X-ray bursts have been observed, implying a burst rate of one per 407 ks (Livingstone et al. 2011). *Bona fide* AXPs have a wide range of observed burst rates, from < 1 burst per ~ 700 ks in 1RXS J170849.0–400910, up to 1 burst per ~ 30 ks for 1E 2259+586.

Finally, a study of the X-ray pulse profile of PSR B1509–58 shows no significant variability on time scales of days to years. Variations in individual pulse profiles are constrained to be less than 2.1% from the average profile at the 3σ level. Together, these results confirm the hypothesis that RPPs can have stable X-ray properties on both short- and long-term time scales.

7.1. Radiative variability from rotation-powered pulsars

Previous studies have shown a correlation between \dot{E} and L_X in the soft X-ray band for magneto-

spheric emission from RPPs and their nebular emission (Seward & Wang 1988; Becker & Trümper 1997; Kargaltsev & Pavlov 2008). This can be interpreted as a constant value of the conversion of spin-down luminosity into X-ray luminosity, $\eta_X = L_X/\dot{E}$, for all RPPs. Establishing a similar correlation between pulsed X-ray luminosity and \dot{E} would be interesting, and implicitly requires L_X to be stable. Prior to this study of PSR B1509–58, the long-term stability of L_X had not been well established for any pulsar, largely owing to systematic uncertainties when comparing results from different telescopes. Here, we show that L_X can be steady on day-to-year-long time scales for RPPs. This confirms the initial hypothesis, and stands in stark contrast to the magnetars, where L_X varies dramatically.

Recent studies have shown that radio emission variability is more common in pulsars than previously thought (e.g. Lyne et al. 2010; Weltevrede et al. 2011). Specifically, the radio emission variability seen in the “intermittent” pulsars (Kramer et al. 2006; Lyne et al. 2010) appears to be associated with large-scale magnetospheric variations. If such a mechanism were active in PSR B1509–58, variations in L_X would be expected, and should be visible in our data, along with variations in the X-ray pulse profile. Because high-energy pulsar emission is more closely associated with the outer magnetosphere, naively, one might expect more dramatic variations in the X-ray regime than in the energetically unimportant radio regime. So far this cannot be confirmed, because none of the “intermittent” pulsars have detectable magnetospheric X-ray pulsations, and no variations in the X-ray pulse profile of PSR B1509–58 were detected here.

Interestingly, two high B -field RPPs, PSR J1846–0258 and J1119–6127, have shown unusual radiative behavior near the time of a rotational glitch, in the X-ray and radio regimes, respectively (Kuiper & Hermsen 2009; Livingstone et al. 2010; Weltevrede et al. 2011). Given this apparent propensity for pulsars with higher-than-average B -fields to display radiative variability and PSR B1509–58’s relatively large magnetic field of 1.5×10^{13} G, future observations of both the radio and X-ray emission properties of PSR B1509–58 may show unusual behavior, particular in the case of a glitch.

7.2. Relationship between B and magnetar outbursts

The exact relationship between the estimated dipole field strength and the ability and/or frequency of a neutron star to exhibit magnetar activity remains to be established. However, there is now a wide range of dipole B estimates in neutron stars exhibiting magnetar outbursts.

Perna & Pons (2011) suggest that all neutron stars may exhibit the type of X-ray outbursts typically associated with magnetars, but that the frequency of events is highly dependent on both the age and the magnetic field strength of the source. For very young neutron stars (< 2 kyr), outbursts may be observed roughly yearly for $B \simeq 8 \times 10^{14}$ G, but only every 50–100 yr for $B \simeq 2 \times 10^{14}$ G. Thus for neutron stars with $B \simeq 10^{13}$ G, such as PSR B1509–58 and PSR J1846–0258, outbursts should be less frequent than once per century. This implies that the observation of an outburst from PSR J1846–0258 was relatively unlikely given that it has only been ob-

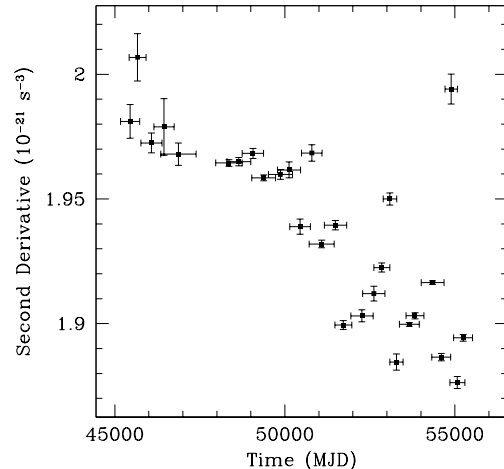


Figure 5. Measurements of $\ddot{\nu}$ from short phase-coherent timing solutions. Data prior to MJD 53000 were previously reported in Livingstone et al. (2005b). A weighted least-squares fit to the data gives a slope of $\ddot{\nu} = 1.21(13) \times 10^{-31} \text{ s}^{-4}$. The effect of timing noise is visible as scatter in the data.

served for ~ 11 yr, and that the lack of magnetic activity from PSR B1509–58 is not surprising. Ongoing observations of many high- B radio pulsars should increase the chances of further observations of magnetar-like bursts from RPPs.

7.3. Braking index, timing noise, and glitches

We presented an extension of the timing solution of PSR B1509–58 from 21.3 yr (Livingstone et al. 2005b) to 28.4 yr. We found a braking index of $n = 2.832(3)$, which is 1.6σ from the value based on 21.3 yr of data.

The scatter in short measurements of $\ddot{\nu}$, and therefore in n , is visible in both Figures 5 and 2, and is typical of timing noise in young pulsars. We observed that the root-mean-square variation in n is 3.5%, larger than the variations observed in the Crab pulsar of $\sim 0.5\%$ (Lyne et al. 1993). We note that there is evidence for timing noise, but no evidence for a glitch, in contrast to the suggestion made by Hobbs et al. (2010) that timing noise in pulsars with characteristic ages less than $\tau_c < 10^5$ yr is entirely because of unmodeled glitch recovery. However, it remains possible that PSR B1509–58 experiences very small glitches that cannot be distinguished from timing noise given the current data.

Because no glitches were found in the latest 7.1 yr of timing data, this extends the time without a detected glitch for PSR B1509–58 to 28.4 yr. While the youngest pulsars ($\tau_c < 2$ kyr) tend to have smaller and fewer glitches than somewhat older pulsars ($\tau_c \sim 5 - 10$ kyr), PSR B1509–58 is extreme in its lack of glitches. For example, the similarly aged Crab pulsar has had 24 glitches in 42 yr of observations, PSR B0540–69 has had one glitch in 7.6 yr, and PSR J1119–6127 has had 3 glitches in 12 yr (Espinoza et al. 2011; Livingstone et al. 2005a; Weltevrede et al. 2011).

A higher order analog to the braking index ($n = \ddot{\nu}\nu/\dot{\nu}^2$), is the “second braking index”, which can be predicted from a measurement of n to be $m_0 \equiv n(2n-1)$ and measured with a value of $\ddot{\nu}$ to be $m = \ddot{\nu}\nu^2/\dot{\nu}^3$. Timing noise and glitches prevent a measurement of n for most pulsars. A measurement of m is even more rare – signif-

icant measurements have only been made for the Crab pulsar and PSR B1509–58 (Lyne et al. 1993; Kaspi et al. 1994; Livingstone et al. 2005b). If the standard spin-down model ($\dot{\nu} = -K\nu^n$) is an accurate description of the spin down of the pulsar, then $m = m_0$. By contrast, $n < 3$ and $m \neq m_0$ implies that $K = K(t)$ and a measurement of m different from m_0 provides constraints on the functional form of $K(t)$ (Blandford & Romani 1988).

Using the full span of available data of 28.4 yr, we found $\dot{\nu} = -1.21(13) \times 10^{-31} \text{ s}^{-4}$, which is within 1σ from the previously reported value based on 21.3 yr of data. For the current measurements of n and $\dot{\nu}$, we find that $m_0 = 13.21 \pm 0.03$ and $m = 17.6 \pm 1.9$, which differ at the 2.3σ level (see Table 1 for all rotational parameters). If uncertainties continue to decrease at the same rate as over the last 7.1 yr since the previous measurement, and the measured value of m remains stable, with another ~ 6 yr of timing observations, the uncertainties should be small enough that m would differ from m_0 at the 3σ level. If this proves to be the case and the two values are inconsistent, this would present challenges to the standard model of pulsar spin-down (e.g., Blandford & Romani 1988; Blandford 1994).

8. CONCLUSIONS

Analyzing 14.7 yr of *RXTE* data, we found no evidence of variability in the X-ray emission of PSR B1509–58. We have placed limits on possible changes in the pulsed flux, profile variability, and burst rate from PSR B1509–58. This indicates that it is indeed possible, as typically assumed, for the X-ray emission properties of RPPs to be stable on day to decade long time scales.

Several RPPs have dipole B estimates close to, or larger than, magnetar-strength fields. These RPPs are typically referred to as the high B -field pulsars. The link between these and magnetars is not well understood and is under investigation (e.g. Olausen et al. 2010; Zhu et al. 2011, 2009; Ng & Kaspi 2010). These pulsars, along with PSR J1846–0258, are possibly related to the transient magnetars (Kaspi & McLaughlin 2005), such as XTE 1810–197 which experience long periods of quiescence, followed by magnetar activity (Ibrahim et al. 2004).

If the internal B field of a neutron star can be much larger than the observed external field responsible for the spin-down (as suggested for SGR 0418+5729; Rea et al. 2010) then it becomes difficult to predict which pulsars may experience a future magnetar-like outburst. Indeed, long-term monitoring observations of PSR J1846–0258 showed that a sudden and dramatic (though temporary) change from a pulsar to a magnetar is possible. Thus X-ray monitoring of pulsars such as that performed with *RXTE* of PSR B1509–58 provides an opportunity to discover future outbursts from less-than-obvious magnetar candidates.

This research made use of data obtained from the High Energy Astrophysics Science Archive Research Center Online Service, provided by the NASA-Goddard Space Flight Center. VMK holds a Canada Research Chair and the Lorne Trottier Chair in Cosmology and Astrophysics. Funding support for this work was provided by an NSERC Discovery Grant and Polanyi Prize, from

FQRNT (Fonds quebécois de la recherche sur la nature et les technologies) via the Centre de Recherche en Astrophysique du Québec (CRAQ), CIFAR (Canadian Institute for Advanced Research) and from a Killam Research Fellowship.

REFERENCES

- Becker, W. & Trümper, J. 1997, *A&A*, 326, 682
 Blandford, R. D. 1994, *MNRAS*, 267, L7
 Blandford, R. D. & Romani, R. W. 1988, *MNRAS*, 234, 57P
 Cusumano, G., Mineo, T., Massaro, E., Nicastro, L., Trussoni, E., Massaglia, S., Hermsen, W., & Kuiper, L. 2001, *A&A*, 375, 397
 Efron, B. 1979, *The Annals of Statistics*, 7, 1
 Espinoza, C. M., Lyne, A. G., Stappers, B. W., & Kramer, M. 2011, *MNRAS*, 414, 1679
 Gaensler, B. M., Brazier, K. T. S., Manchester, R. N., Johnston, S., & Green, A. J. 1999, *MNRAS*, 305, 724
 Gavril, F. P., Gonzalez, M. E., Gotthelf, E. V., Kaspi, V. M., Livingstone, M. A., & Woods, P. M. 2008, *Science*, 319, 1802
 Gavril, F. P., Kaspi, V. M., & Woods, P. M. 2004, *ApJ*, 607, 959
 Hobbs, G., Lyne, A. G., & Kramer, M. 2010, *MNRAS*, 402, 1027
 Ibrahim, A. I., Markwardt, C. B., Swank, J. H., Ransom, S., Roberts, M., Kaspi, V., Woods, P. M., Safi-Harb, S., Balman, S., Parke, W. C., Kouveliotou, C., Hurley, K., & Cline, T. 2004, *ApJ*, 609, L21
 Jahoda, K., Markwardt, C. B., Radeva, Y., Rots, A. H., Stark, M. J., Swank, J. H., Strohmayer, T. E., & Zhang, W. 2006, *ApJS*, 163, 401
 Jahoda, K., Swank, J. H., Giles, A. B., Stark, M. J., Strohmayer, T., Zhang, W., & Morgan, E. H. 1996, *Proc. SPIE*, 2808, 59
 Kargaltsev, O. & Pavlov, G. G. 2008, in *American Institute of Physics Conference Series*, Vol. 983, 40 Years of Pulsars: Millisecond Pulsars, Magnetars and More, ed. C. Bassa, Z. Wang, A. Cumming, & V. M. Kaspi, 171–185
 Kaspi, V. M. 2007, *Astrophys. Space Sci.*, 308, 1
 Kaspi, V. M. 2010, *Proceedings of the National Academy of Science*, 107, 7147
 Kaspi, V. M., Manchester, R. N., Siegelman, B., Johnston, S., & Lyne, A. G. 1994, *ApJ*, 422, L83
 Kaspi, V. M. & McLaughlin, M. A. 2005, *ApJ*, 618
 Kramer, M., Lyne, A. G., O’Brien, J. T., Jordan, C. A., & Lorimer, D. R. 2006, *Science*, 312, 549
 Kuiper, L. & Hermsen, W. 2009, *A & A*, 501, 1031
 Kumar, H. S. & Safi-Harb, S. 2008, *ApJL*, 678, L43
 Livingstone, M. A., Kaspi, V. M., & Gavril, F. P. 2005a, *ApJ*, 633, 1095
 —. 2010, *ApJ*, 710, 1710
 Livingstone, M. A., Kaspi, V. M., Gavril, F. P., & Manchester, R. N. 2005b, *ApJ*, 619, 1046
 Livingstone, M. A., Ng, C.-Y., Kaspi, V. M., Gavril, F. P., & Gotthelf, E. V. 2011, *ApJ*, 730, 66
 Lyne, A., Hobbs, G., Kramer, M., Stairs, I., & Stappers, B. 2010, *Science*, 329, 408
 Lyne, A. G., Pritchard, R. S., & Smith, F. G. 1993, *MNRAS*, 265, 1003
 Manchester, R. N. & Taylor, J. H. 1977, *Pulsars* (San Francisco: Freeman)
 Marsden, D., Blanco, P. R., Gruber, D. E., Heindl, W. A., Pelling, M. R., Peterson, L. E., Rothschild, R. E., Rots, A. H., Jahoda, K., & Macomb, D. J. 1997, *ApJ*, 491, L39
 Mereghetti, S. 2008, *A&A Rev.*, 15, 225
 Ng, C. Y. & Kaspi, V. M. 2010, *arXiv:1010.4592*
 Olausen, S. A., Kaspi, V. M., Lyne, A. G., & Kramer, M. 2010, *ApJ*, 725, 985
 Perna, R. & Pons, J. A. 2011, *ApJ*, 727, L51+
 Rea, N. & Esposito, P. 2011, in *High-Energy Emission from Pulsars and their Systems*, eds. D. F. Torres & N. Rea, 247
 Rea, N., Esposito, P., Turolla, R., Israel, G. L., Zane, S., Stella, L., Mereghetti, S., Tiengo, A., Götz, D., Göğüş, E., & Kouveliotou, C. 2010, *Science*, 330, 944
 Rots, A. H., Jahoda, K., Macomb, D. J., Kawai, N., Saito, Y., Kaspi, V. M., Lyne, A. G., Manchester, R. N., Backer, D. C., Somers, A. L., Marsden, D., & Rothschild, R. E. 1998, *ApJ*, 501, 749

Table 1
X-ray Spin Parameters for PSR B1509–58

Parameters for phase-coherent analysis	
Dates (Modified Julian Day)	50148.096 – 55521.082
Epoch (Modified Julian Day)	52834.589000
N_{TOA}	188
ν (Hz)	6.611515243850(3)
$\dot{\nu}$ (10^{-11} s^{-2})	–6.694371307(6)
$\ddot{\nu}$ (10^{-21} s^{-3})	1.9185594(5)
$\ddot{\nu}$ (10^{-31} s^{-4})	–0.9139(2)
Parameters for partially coherent analysis	
Average Braking Index, n	2.832(3)
$m_0 \equiv n(2n - 1)$	13.21(3)
$\ddot{\nu}$ (10^{-31} s^{-4})	–1.21(13)
Second braking index, m	17.6(1.9)

Note. — Spin parameters for 14.7 yr of X-ray timing data for PSR B1509–58.

Table 2
Partially coherent ephemerides

Epoch (MJD)	ν (Hz)	$\dot{\nu}$ (10^{-11} Hz^{-2})	$\ddot{\nu}$ (10^{-21} Hz^{-3})	Date range (MJD)
50448	6.6253600487(2)	–6.734167(2)	1.939(3)	50148–50749
51083	6.6216683438(2)	–6.7234900(8)	1.932(2)	50750–51449
51853	6.6171996051(2)	–6.710680(1)	1.917(3)	51470–52167
52616	6.6127798918(2)	–6.698028(1)	1.912(3)	52265–52926
53091	6.6100326310(1)	–6.6901006(7)	1.950(2)	52893–53289
53647	6.60682103661(5)	–6.6809030(3)	1.9032(6)	53311–53982
54345	6.60279542362(6)	–6.6694306(4)	1.9165(7)	54007–54681
54892	6.5996455256(2)	–6.660372(2)	1.994(6)	54707–55076
55241	6.5976380501(1)	–6.6546543(5)	1.894(1)	54960–55522

Note. — Uncertainties are formal TEMPO uncertainties. These spin parameters are used for the pulsed flux analysis; see Section 4.

Table 3
Minimum burst fluences to detect bursts

Time resolution (ms)	Total counts	Counts/PCU	Burst fluence ($10^{-12} \text{ erg cm}^{-2}$)
15.625	20	7	2.6
31.25	25	8	5.9
62.25	30	10	15
125.0	40	13	39

Note. — All fluences are for the 2–20 keV energy range. Fluences are determined from the simulations described in Section 6.

Seward, F. D. & Harnden Jr., F. R. 1982, ApJ, 256, L45
 Seward, F. D. & Wang, Z.-R. 1988, ApJ, 332, 199
 Thompson, C. & Duncan, R. C. 1996, ApJ, 473, 322
 Thompson, C., Lyutikov, M., & Kulkarni, S. R. 2002, ApJ, 574, 332
 Weltevrede, P., Johnston, S., & Espinoza, C. M. 2011, MNRAS, 411, 1917
 Woods, P. M. & Thompson, C. 2006, in Compact Stellar X-ray Sources, ed. W. H. G. Lewin & M. van der Klis (UK: Cambridge University Press)

Zhu, W., Kaspi, V. M., Gonzalez, M. E., & Lyne, A. G. 2009, ApJ, 704, 1321
 Zhu, W. W., Kaspi, V. M., McLaughlin, M. A., Pavlov, G. G., Ng, C.-Y., Manchester, R. N., Gaensler, B. M., & Woods, P. M. 2011, ApJ, 734, 44